Computers and Electronics in Agriculture 79 (2011) 216–225

Contents lists available at SciVerse ScienceDirect

Computers and Electronics in Agriculture

journal homepage: www.elsevier.com/locate/compag

Development of a row guidance system for an autonomous robot for white asparagus harvesting

Fuhong Dong *, Wolfgang Heinemann, Roland Kasper

Institute of Mobile Systems (IMS), Faculty of Mechanical Engineering, Otto-von-Guericke University Magdeburg, Universitätsplatz 2, D-39106 Magdeburg, Germany

ARTICLE INFO

Article history:
Received 16 May 2011
Received in revised form 17 August 2011
Accepted 4 October 2011

Keywords:
Agricultural robot
Row guidance
White asparagus harvesting
Cascade control
Differential drive

ABSTRACT

The special cultivation features of white asparagus pose new challenges to the research and development of the row guidance control. This paper presents a row tracking system of a two-layer structure for an autonomous robot developed to harvest white asparagus. At the low level, two independent speed control loops are suggested to ensure the actual revolutions of the drive motors to follow their demanded values. A cascade control structure, consisting of an inner orientation error controller and an outer lateral offset controller, is proposed for the high level to drive the robot to track the desired trajectory. The most important advantage of the cascade structure is that the inner loop directly regulates the most significant error (the orientation error), which minimizes the impact of the external disturbances upon the outer loop. Moreover, the cascade scheme allows the orientation angle to be limited within a given range. That ensures a collision-free tracking. The controllers are designed based on the traditional proportional-integral-derivative (PID) algorithms. The control parameters are selected by using root locus analysis, which guarantees the system stability. The effectiveness of the proposed control regime is evaluated by numerical simulations and validated by experiments. The experimental results demonstrate that with the suggested row guidance strategy a satisfactory tracking accuracy of ±0.5 cm is achieved.

1. Introduction

1.1. Cultivation and harvest of white asparagus

White asparagus is one of the most favorite vegetables in Germany and well-known as "the royal vegetable". In 2010, approximately 92,400 tons of asparagus is harvested on 18,800 hectares in Germany (Bonn, 2011). The cultivation is expected to continue to expand. White asparagus is cultivated in parallel trapezoidal mounds, which are heaped knee-highly around the plants. Each mound is covered with a plastic film (see Fig. 1). To harvest the stalks manually, the workers move firstly the film aside, cut stalks off with a special knife one by one, push the soil back and replace the film on the mound at the end. When the harvesters cut asparagus, care must be taken not to damage the shorter developing spears under the ground. The stalks need to be cut shortly after their spears emerge from the mound. Otherwise the tips will turn into light purple color, which decreases the product quality and results in significantly lower selling price (European Commission, 1999). The harvesting time of white asparagus generally begins from early or mid-April and ends on June 24 every year. During these 10 weeks, the asparagus is generally harvested twice a day.

White asparagus harvesting is a highly repetitive and labor intensive task that is typically done manually at present. With the cultivation area expanding, it becomes increasingly difficult to employ adequate workers during the harvesting season. Besides, the labor cost is getting increasingly higher (Leibniz-Institute of Agricultural Engineering, 2010). Therefore, it is essential and urgent to explore an automated solution for white asparagus harvesting to release workers from the laborious manual task and to lower the production cost (Geyer et al., 2005). It is worth noting that the successfully used harvester for green asparagus harvesting developed by Arndt et al. (1997) is not suitable for the white asparagus harvesting due to the special cultivation features of white asparagus. In recent years, engineers have been attempting to mechanize the harvesting process of white asparagus and significant progress has been achieved. One of the earliest asparagus harvesting assistant machines named AspergeSpin A1 (Wonneberge, 2005) was developed by ENGELS MACHINES Innovatietechniek company, Holland. AspergeSpin A1, which is also popularly used at present, assists workers in film lifting, replacing and also carrying the asparagus containers. In June 2008, the French company Firma Kirpy presented a non-selective harvesting machine Type RGA (Uwihs, 2008) for white asparagus. Type RGA is dragged by a tractor. It cuts through the asparagus mound completely and then transfers the harvested asparagus spears together with the soil over a sieve band in sequence. The asparagus mound is then

* Corresponding author. Tel.: +49 391 67 11712; fax: +49 391 67 12656.
E-mail address: fuhong.dong@ovgu.de (F. Dong).

0168-1699/$ - see front matter © 2011 Elsevier B.V. All rights reserved.
doi:10.1016/j.compag.2011.10.002

Nomenclature

B_m	viscous friction coefficient drive motor (N m s rad^{-1})
e_S	lateral offset front ultrasonic sensor (m)
e_y	lateral offset mobile robot (m)
e_θ	orientation error mobile robot (rad)
e_{y0}, $e_{\theta 0}$	initial position error mobile robot (m), (rad)
g	gear ratio chain gearbox (–)
G_{mPI}	transfer function PI motor speed controller (–)
G_{mcl}	transfer function closed-loop motor speed controller (–)
G_{PDy}	transfer function PD lateral displacement controller (–)
J_m	motor inertia with its wheel (kg m^2)
K_e	back-emf constant (V s)
$k_{p\omega}$, $k_{i\omega}$	proportional and integral gains of G_{mPI} (V s rad^{-1}), (V s rad^{-1})
K_m	torque constant motor (N m A^{-1})
k_{ms}	simplified gain of G_{mcl}
k_{py},k_{dy}	proportional and derivative gains of G_{PDy}
$k_{p\theta}$	proportional gain orientation controller (s^{-1})
L_a, L_b	length and width mobile robot base (m), (m)
L_m	inductance drive motor (H)
R_m	motor resistance (Ohm)
r	radius drive wheel (m)
n_{ref}	desired motor speed (rpm), equivalent to $n_{ref} = \frac{30}{\pi \cdot r} \cdot v_{ref}$
S_f, S_r	front and rear side distances (m), (m)
S_{f0}, S_{r0}	initial values of side distances S_f and S_r, (m), (m)
S_{ref}	desired side distance (m)
T_{ms}	simplified time constant of G_{mcl} (s)
u	motor supply voltage (V)
u_L,u_R	supply voltages for left and right drive motors (V), (V)
v	actual forward linear velocity mobile robot (m s^{-1})
v_L,v_R	actual linear velocities left and right wheels (m s^{-1}), (m s^{-1})
v_{ref}	desired forward linear velocity mobile robot (m s^{-1})
ω	actual angular speed mobile robot (rad s^{-1})
ω_{mdiff}	differential angular speed to steer the vehicle (rad s^{-1})
ω_{ml}, ω_{mr}	actual revolutions left and right motors (rad s^{-1}), (rad s^{-1})
ω^*_{ml}, ω^*_{mr}	desired revolutions left and right motors (rad s^{-1}), (rad s^{-1})
ω_{mref}	desired motor angular speed (rad s^{-1}), given by $\omega_{mref} = \frac{g}{r} \cdot v_{ref}$
y	actual lateral displacement (m)
y_d	desired lateral displacement (m)
θ	actual heading direction (rad)
θ_d	desired heading direction of the robot (rad)
θ_{ref}	reference heading angle given by lateral offset controller (rad)

reformed automatically. The full harvesting machine greatly improves the productivity and relieves the manual task. However, it significantly reduces the output and quality of the products because the shoots that are developing under the surface are also non-selectively harvested at a time. In 2008, the German company ASM DIMANTEC invented a semi-automatic machine named Spargel-Panther (Peiter, 2008). Spargel-Panther is a tractor driven machine designed to harvest asparagus for three cultivation beds. With the help of a laser beam, the driver can locate the position of each asparagus tip by operating a joystick. The consequent harvesting procedure is automatically performed in series, which consists of coordinating the position of the harvesting equipment, cutting off the asparagus under the ground with a certain depth, moving the shoot out with a gripper and transferring it into containers. The Dutch company Brabantse Wal presented the first prototype of a full-automatic asparagus harvester in the world in 2008 (Lindhout, 2008). Although the above companies have made pioneering endeavors, the detailed research and development information is unavailable due to commercial reasons. In the academic community only Chatzimichali et al. (2009) have recently outlined a conceptual design of an advanced prototype robot for automatic white asparagus harvesting. In their work, the structure of the prototype robot consisting of a caterpillar drive system, asparagus identification and harvesting system has been detailed. The realization of the proposed design is still ongoing. To the best of our knowledge, there is no other public research report about full automatic machine for the selective harvesting of white asparagus at present.

To automate the harvesting process for white asparagus, two primary requirements must be suited: automated row guidance and reaping asparagus automatically. In this paper, we concentrate on the development of a row guidance system for an autonomous asparagus harvesting mobile robot driven by an electrical system, and our objective is to develop a guidance control design suitable for the application in white asparagus harvesting. Our ultimate goal is to design a full autonomous robot for white asparagus harvesting (see Fig 2).

Fig. 1. Cultivation mounds of white asparagus and manual harvesting work.

Fig. 2. Mobile robot for white asparagus harvesting in field.

1.2. Automatic guidance system

In recent decades, the development of technologies such as machine vision analysis, global positioning systems (GPS) and robotics allows the improvement of automatic vehicle guidance. Machine vision and GPS are most widely used for the row guidance control. Various vision-based guidance systems have been proposed for the field machine to perform weeding, cultivating, chemical spraying and harvesting (Åstrand and Baerveldt, 2002; Benson et al., 2003; Tillett et al., 2002). The most commonly used method based on machine-vision to identify crop rows is the Hough transform (Hough, 1962), which is a computationally efficient procedure and capable of dealing with the situations where the crop stand is incomplete with gaps in the crops. In vision based applications, a real-time imagery processing is essential to separate objects of interest from field images, which is a serious challenge for the processing device to execute complex image processing algorithms. Moreover, the effectiveness of the vision system is affected by lighting conditions and background interference (Slaughter et al., 2008). Alternatively, the Real-Time Kinematic GPS (RTK GPS) with precision of a few centimeters is commercially available for some tractors. Stoll and Kutzbach (2000) developed an automatic steering system for a self-propelled forage harvester using RTK GPS as the only positioning sensor. Kise et al. (2002) proposed an RTK GPS guidance system for a field autonomous vehicle traveling along a curved path with a maximal tracking error of 13 cm. To use the RTK GPS method, a reference receiver (Base) must be placed on a known reference point, and a roving receiver (Remote) on the vehicle. The Base transmits measurement or correction information through a radio link to the Remote. The Base and Remote must communicate with each other at all times during vehicle operation in order to maintain good accuracy. This guidance method suffers from some limitations. It is difficult to guarantee consistent positioning accuracy for varied field conditions. Another drawback is the inherent time delay (Li et al., 2009). Besides, pre-investment required for the Base and Remote devices is generally considerably high for the agricultural applications (Buick, 2006).

In this study, we introduce firstly the mechanical design of our autonomous mobile robot platform for white asparagus harvesting (see Fig. 2). For our robot platform, the objective of the guidance control system is set so that the vehicle does not damage any asparagus bed by driving too close to it. For this purpose, a low-cost row guidance system is proposed for the harvesting application in the white asparagus field. The actual in-row position of the vehicle with respect to the asparagus bed is derived by the front and rear side distances, which are measured by two ultrasonic sensors. A two-layer architecture for the guidance control is used to reject the internal and external disturbances. At the low level two independent speed controllers are employed to make the drive motors rotate at the reference speeds supplied by the trajectory controller at the high level. A cascade control system, which is composed of main control loop of lateral offset and the auxiliary loop of orientation error, is especially suggested at the high level to reduce the influence of external disturbances to the lowest level. Finally, simulations and experiments are performed to evaluate the tracking performance of the proposed strategy.

The rest of this work is organized as follows. We start with the mechanical design of the harvesting robot in the next section. Section 3.1 describes the vehicle kinematics. Section 3.2 is devoted to quantifying the tracking error using the front and rear side distances. In Section 4.1, we present a row tracking system based on cascade control method. The control system design is presented in detail in Section 4.2. Section 5 shows the simulation and experimental tracking performance for the robot with different initial tracking errors, and relevant discussions are drawn subsequently. Finally, we close with a brief concluding remarks and future work in Section 6.

2. Mechanical description of the vehicle platform

White asparagus is cultivated in parallel beds that have a trapezoidal cross-section and are raised up over the field surface up to 50 cm tall. The width of the asparagus bed is about 1 m wide at the bottom, and the in-row space is approximately 80 cm. We designed an autonomous harvesting robot platform for both efficiency and cost effectiveness. The mechanical design is shown in Fig. 3. The robot base has dimensions of 3.1 × 1.8 × 1.6 m ($l/w/h$) and a weight without load up to 450 kg, and its center of mass is located slightly behind of the front axis. The vehicle chassis is composed of two motors, transmission elements, electronics, sensors and two 12 V batteries. The robot platform is a differential drive vehicle and has two drive wheels with same radius of 30 cm at the front. The drive wheels are actuated independently by two 450 W DC motors supplied with 24 V voltage. The nominal torque of the motor is 12.6 Nm. The shaft of each motor is connected with its wheel through a chain gear box with a reduction ratio of 16:1. Two casters with radius of 15 cm are installed at the rear to provide balance. Motor speed is sensed through an incremental optical encoder. Two ultrasonic sensors are installed on the right side of the harvester to measure the front and rear side distances with respect to its tracking row. One of them is near the front wheel and the other near the rear one. Measurements of the sensors are fed back to the controllers. The advantage of ultrasonic sensor over vision system is that the effectiveness of its measurement is not affected by lighting conditions and background interference. It also improves computational efficiency and lowers the cost of the harvester. The robot platform is also equipped with a film roller at the front, and through a sliding channel the film is replaced behind the vehicle automatically. The robot can be steered only by maneuvering the relative speeds of the drive wheels.

3. Kinematics and description of tracking deviation

3.1. Kinematics

The vehicle platform is assumed to be composed of rigid bodies and to move on a planar surface. As the operating velocity of the robot is limited to 5 km/h, it is supposed that the wheels are non-deformable and that there is no translational or lateral slip between the wheels and the ground surface. The translational velocities of the left and right wheels are obtained by $v_L = \omega_{ml} r/g$ and $v_R = \omega_{mr} r/g$, where ω_{ml} and ω_{mr} are angular speeds of the left and right drive motors, r the radius of the drive wheel and g the reduction ratio of the chain gearbox. The center point P (see Fig. 4) of the axle of the driving wheels is defined as the reference point of the mobile robot position. The forward linear velocity v and angular

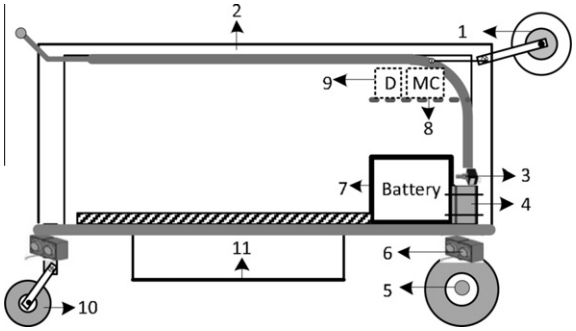

Fig. 3. Mechanical design of the mobile robot (1. Film roller, 2. Sliding channel for the film, 3. Incremental optical encoder, 4. DC motor 5. Front drive wheel, 6. Ultrasonic sensor, 7. Battery, 8. Micro-controller, 9. Drive board, 10. Caster/rear wheel, and 11. Loading platform).

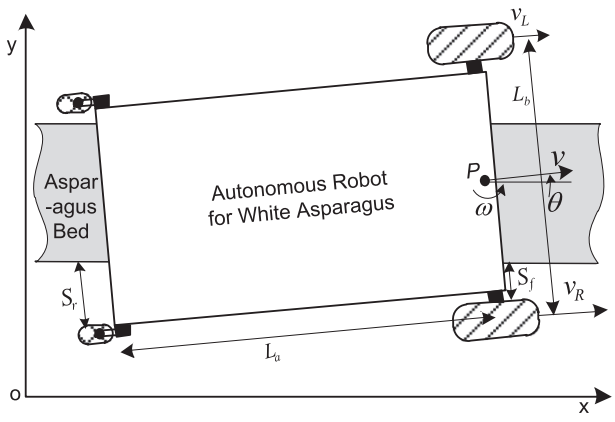

Fig. 4. Top view of the asparagus harvesting robot.

speed ω at the point P can be described in the moving frame as follows:

$$v = \frac{v_R + v_L}{2} \tag{1}$$

$$\omega = \frac{v_R - v_L}{L_b} \tag{2}$$

where L_b is the distance between the two drive wheels.

For the sake of convenience, the X axis of the base frame is defined in parallel to the asparagus bed pointing right. In the base frame, the kinematic model of the differential drive mobile robot can be expressed as (Siegwart and Nourbakhsh, 2004):

$$\begin{pmatrix} \dot{x} \\ \dot{y} \\ \dot{\theta} \end{pmatrix} = \begin{pmatrix} cos\theta & 0 \\ sin\theta & 0 \\ 0 & 1 \end{pmatrix} \begin{pmatrix} v \\ \omega \end{pmatrix} \tag{3}$$

where x, y and θ are the positions and orientation of the robot, $\dot{x}$, $\dot{y}$ and $\dot{\theta}$ are their derivatives and represent the velocities and angular speed of the vehicle, respectively.

3.2. Tracking deviation from the tracking row

In order to follow crop rows, it is necessary to determine the vehicle position with respect to the target row. The desired and actual positions are illustrated in Fig. 5 by the dashed and solid rectangular frames, respectively. The tracking deviation of the robot from the target asparagus row can then be described using the lateral offset e_y and orientation error e_θ:

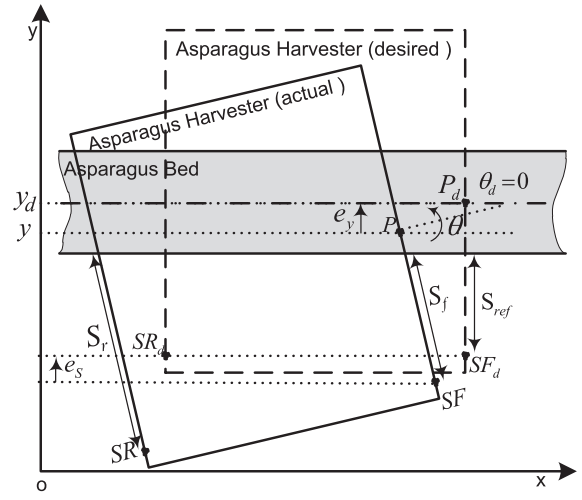

Fig. 5. Graphic representation of the tracking deviation.

$$e_y = y_d - y, \quad e_\theta = \theta_d - \theta \tag{4}$$

where y_d and θ_d are the desired lateral displacement and heading angle whose values are both zero in this work, i.e. $y_d = 0$, $\theta_d = 0$.

The actual orientation and lateral displacement of the harvesting robot are computed using the front and rear side distances measured by the two ultrasonic sensors *SF* and *SR* also shown in Fig. 5. According to the geometric relations, the actual orientation θ can be calculated using the side distances S_f and S_r as follows:

$$\theta = \arctan\frac{S_f - S_r}{L_a} \tag{5}$$

where L_a is the length of the robot base. The actual lateral displacement y is given by

$$y = e_S + sign(e_S)\,\frac{L_b}{2}\,(1 - \cos\theta) \tag{6}$$

$$e_S = S_{ref} - S_f \cos\theta \tag{7}$$

where S_{ref} represents the reference side distance for the ultrasonic sensors and corresponds to the side distances for the vehicle by $e_y = 0$ and $e_\theta = 0$, e_S the actual lateral deviation of SF.

The actual lateral displacement y and the heading angle θ are fed back to the trajectory controller at the high level to generate the desired speeds for the drive motors. Considering that the asparagus beds are composed generally of linear segments and extremely soft arcs, the direction deviation of the tracking row is within 3°. Therefore, it is reasonable to make an approximation of $\sin\theta \approx \theta$. The tracking deviation of the mobile robot from the aimed trajectory can be rewritten as:

$$\dot{y} = v\theta \tag{8}$$

$$\dot{\theta} = \omega \tag{9}$$

4. Row guidance control design

Differential drive robots have restricted motion due to their nonholonomic constraints. To ensure the global stability for any arbitrary trajectory, considerable nonlinear control techniques have been suggested. The more often employed strategies are based on the nonlinear state feedback (Aguilar et al., 1998; Chwa, 2010; d'Andréa-Novel et al., 1995; Zhang et al., 1997), adaptive control (Colbaugh et al., 1998; Mazur, 1997), model-based predictive control (Klančar and Škrjanc, 2007) and intelligent control method like fuzzy logic (Espinosa et al., 2001; Tso et al., 1996). However, the nonlinear control methods are usually quite complicated in applications and the computation effort is too large to be implemented on an economic micro-controller in real-time (Chwa, 2010), although rigorous analysis has been performed for the controller development to guarantee the system stability. Therefore, from the viewpoint of a practical application, it is desirable to adopt the PID controllers (Chwa, 2010). Borges et al. (2000) proposed a P controller based on feedback trajectory control design for an automated mobile robot in laboratory. Marchant et al. (1997) suggested a simple PD controller for the row following system of an autonomous vision-guided agricultural vehicle. With the PD controller, the agricultural vehicle tracked the target trajectory with satisfying performance. The row guidance control for our harvesting robot is designed based upon the conventional PID algorithms.

4.1. Control architecture

The two-layer control structure shown in Fig. 6 is composed of a trajectory control system at the high level and a wheel speed control system at the low level. In this figure, the thin black arrows represent the electrical signal routes and the thick left and right

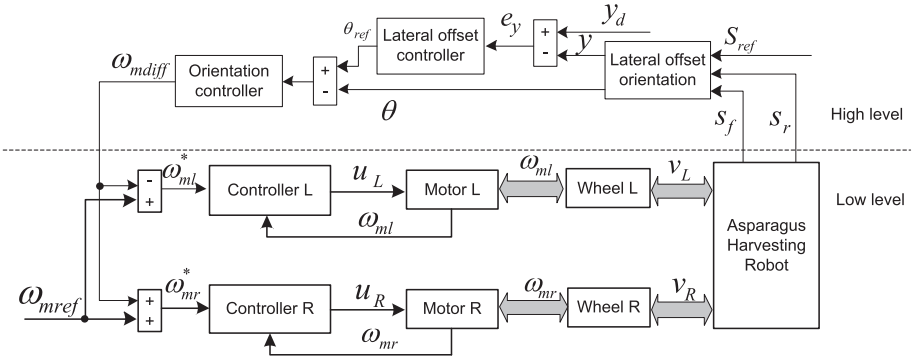

Fig. 6. Block diagram of the row guidance control structure.

arrows in gray represent the mechanical connections. The trajectory controller at the high level with a cascade structure supervises the tracking error, which is calculated using the front and rear side distances S_f and S_r. According to the actual tracking error, the lateral offset controller in the outer loop adjusts the set-point θ_{ref} of the inner loop in real-time. The orientation controller then generates the differential term for the motor speeds to adjust the orientation angle θ. The speed control system at the low level is composed of two individual speed control loops for the drive motors, illustrated by Motor L and Motor R in Fig. 6. The speed loops are employed to ensure that the actual motor speed ω_m always follows the desired speed ω^*_m. The reference angular speeds of the motors are formulated as follows:

$$\omega^*_{ml} = \omega_{ref} - \omega_{mdiff} \tag{10}$$

$$\omega^*_{mr} = \omega_{ref} + \omega_{mdiff} \tag{11}$$

where ω^*_{ml} and ω^*_{mr} are the desired angular speeds for the left and right motors, respectively. Each desired speed consists of two components: a primary angular speed ω_{mref} and a differential term ω_{mdiff}. ω_{mref} is equivalent to the desired forward linear velocity v_{ref} given by $\omega_{mref} = v_{ref}g/r$. ω_{mdiff} is determined by the orientation controller at the high level and used to compensate the tracking error. If the tracking error is zero, i.e. $e_y = 0$ and $e_\theta = 0$, then $\omega_{mdiff} = 0$. The vehicle drives straightly forward with the motors operating at the same speed. Otherwise, by $\omega_{ref} \neq 0$ the trajectory controller is activated. The machine then orients itself through the adjustment of the motor speeds simultaneously to eliminate the tracking error.

As for the tracking control of the differential drive mobile robots, the orientation error e_θ is more sensitive and has the significant impact on the tracking error, because the lateral error e_y depends on e_θ and its time increment. Moreover, e_θ is a direct result of the external disturbances. Therefore, the cascade system suggested for the trajectory system is advantageous in that it suppresses the effect of the external disturbances on the primary process variable e_y. As compared with the guidance control design with a single controller (Borges et al., 2000; Marchant et al., 1997), the cascade structure enables the heading angle θ to be restricted through limiting the output of the lateral offset controller. Accordingly, the violent sway of the rear part of the robot is avoided during the adjustment of the tracking controller. This makes the movement of the robot more stable, which is at the expense of the convergence time of the tracking error.

4.2. Controller design

The speed controller is of proportional-integral type and represented as

$$G_{mPI} = k_{p\omega} + \frac{k_{i\omega}}{s} \tag{12}$$

where $k_{p\omega}$ and $k_{i\omega}$ are the proportional and integral gains, respectively. The open loop transfer function of the motor from the rotational speed ω_m to the input voltage u is

$$\frac{\omega_m}{u} = \frac{K_e}{J_m L_m s^2 + (L_m B_m + J_m R_m)s + B_m R_m + K_e K_m} \tag{13}$$

where L_m is the motor inductance, R_m the motor resistance, B_m the viscous friction coefficient and J_m the equivalent motor inertia together with its drive wheel. K_e and K_m are the motor voltage constant and torque constant, respectively.

The resulting closed-loop transfer function of the speed loop is given by:

$$G_{mcl} = \frac{K_e(k_{p\omega}s + k_{i\omega})}{J_m L_m s^3 + (L_m B_m + J_m R_m)s^2 + (k_{p\omega}K_e + B_m R_m + K_e K_m)s + k_{i\omega}K_e} \tag{14}$$

To simplify the controller design at the high level, the three-order model in Eq. (14) is replaced with an approximate first-order system with time-delay given in Eq. (15).

$$\frac{\omega_m}{\omega^*_m} = \frac{k_{ms}}{T_{ms}s + 1} \tag{15}$$

where k_{ms} is the equivalent loop gain, and T_{ms} the equivalent delay time. Note that this approximation is made only to design the controllers at the high level, and in the simulation studies the original motor speed system is still adopted.

As the time constant of the dynamics is considerably smaller than that of the row tracking system, the transient response of the motor speed was neglected in the trajectory controller design, and the expression $\omega_m = \omega^*_m$ holds. The forward linear velocity v is considered as constant and equals to v_{ref} according to the steering strategy given by Eqs. (10) and (11). The tracking deviation can be expressed as follows:

$$\dot{y} = v\theta \tag{16}$$

$$\dot{\theta} = \frac{r}{L_b g}(\omega_{mr} - \omega_{mr}) \tag{17}$$

It is seen from Eqs. (16) and (17) that the heading angle θ can be regulated only by the differential speed of the right and left motors and that the lateral displacement y can be adjusted only by the heading angle θ.

The open-loop transfer function of the orientation system contributes the integral role. With a proportional controller, the objective of a zero steady-state error can be achieved for the orientation angle control. With the proportional gain $k_{p\theta}$ the closed-loop transfer function of the orientation control system is derived as:

$$\frac{\theta}{\theta_{ref}} = \frac{k_{p\theta}k_{ms}r}{L_b T_{ms} g s^2 + L_b g s + k_{p\theta}k_{ms}r} \tag{18}$$

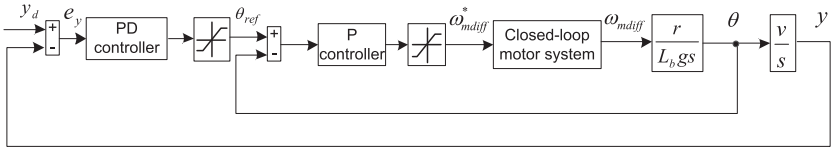

Fig. 7. Block diagram of the cascade tracking control system.

Table 1
Simulation and experimental parameters.

Parameter	Value
Wheel radius r (m)	0.3
Gear ratio g (–)	16:1
Vehicle width L_b (m)	2.1
Supply voltage u (V)	24
Motor inertia J_m (kg m^2)	0.0738
Motor inductance L_m (H)	1×10^{-4}
Viscous friction coefficient B_m (N m s rad^{-1})	4.3×10^{-3}
Back-emf constant K_e (V s rad^{-1})	0.45
Torque constant K_m (N m A^{-1})	0.45
Simplified gain motor closed-loop speed controller $k_m s$ (–)	1
Simplified time constant motor closed-loop speed controller T_{ms} (s)	0.137
Proportional gain orientation controller $k_{p\theta}$ (s^{-1})	204
Proportional gain lateral controller k_{ky} (rad m^{-1})	10
Integral gain lateral controller k_{dy} (rad m^{-1})	3

The lateral offset controller is of a proportional-derivative type and represented as:

$$G_{PDy} = k_{py} + k_{dy}s \tag{19}$$

where k_{py} and k_{dy} are the proportional and derivative gains. The resulting transfer function of the closed-loop system is

$$\frac{y}{y_d} = \frac{k_{p\theta}k_{ms}rv(k_{dy}s + k_{py})}{L_bT_{ms}gs^3 + L_bgs^2 + k_{p\theta}k_{ms}r(1 + k_{dy}v)s + k_{py}k_{p\theta}k_{ms}rv} \tag{20}$$

The block diagram of the simulation system is illustrated in Fig. 7. Parameters of the controllers were selected for the response of the system dynamics with neither overshoot nor steady state error based upon the root locus analysis. The parameters of the robot are collected in Table 1, where the parameters of the drive motor were determined experimentally.

5. Results and discussion

5.1. Simulation studies

Numerical simulations were carried out to evaluate the tracking performance of the proposed control design. An accurate simulation model capable of capturing kinematics of the mobile robot base is established in MATLAB/Simulink. Considering the limitations of the working space and the nonholonomic constraints of the movement of the differential drive mobile robot, a few constraints were imposed on the guidance system. The initial position of the robot is limited by the constraint given in Eq. (21). This is achieved by adjusting the posture of the robot before its startup.

$$|e_{y0}| \leqslant 5 \text{ cm}, \ |e_{\theta 0}| \leqslant 2^0 \tag{21}$$

A more stringent constraint given in Eq. (22) was imposed on the orientation angle to avoid any possible collision between the vehicle and asparagus rows, which is realized through limiting the output of the lateral offset controller.

$$|e_\theta| \leqslant 1.53^0, \text{ i.e. } |S_f - S_r| \leqslant 8 \text{ cm} \tag{22}$$

It is worth noting that in the applications of the field robots, any sudden change in the wheel speed can cause uncontrollable movement of the vehicle due to the inertial force and skidding. Therefore, the differential term ω_{mdiff} is limited to 0.523 rad/s to avoid the slippage of the wheels. Note that the actual position (y, θ) of the robot were established by using pseudo-measurements of the ultrasonic sensors according to Eqs. (5) and (6) in the simulation studies.

A number of simulation studies were repeatedly conducted to evaluate the tracking performance of the proposed row guidance controller. Two group simulation studies of different desired velocities v_{ref} with four representative initial errors were demonstrated. In the two groups, v_{ref} was specified as 0.12 m/s (n_{ref} = 60 rpm) and 0.16 m/s (n_{ref} = 80 rpm), respectively. In the first group the robot started up with two different initial trajectory errors of $(e_{y0}, e_{\theta 0}) = (5.04 \text{ cm}, -1.33^\circ)$ and $(e_{y0}, e_{\theta 0}) = (-3 \text{ cm}, -0.57^\circ)$. A lateral deviation of 1 cm from the target row was introduced at 40s to examine the performance of the guidance controller in terms of the external disturbance. The tracking performance is shown in Fig. 8. In the second group, the robot started up from two different initial positions of $(e_{y0}, e_{\theta 0}) = (5.04 \text{ cm}, -1.33^\circ)$ and $(e_{y0}, e_{\theta 0}) = (-4 \text{ cm}, -2.05^\circ)$. The tracking profiles are illustrated in Fig. 9. For each case, the vehicle is required to converge to the desired trajectory of $(e_{y0}, e_{\theta 0}) = (0 \text{ cm}, 0^\circ)$, i.e. $(S_{fd}, S_{rd}) = (30 \text{ cm}, 30 \text{ cm})$.

From the simulation results illustrated in Figs. 8 and 9, some conclusions are drawn as follows:

The regulation process of the initial tracking error is divided into three stages. In the first stage, the orientation error e_θ is adjusted to its boundary in that the inner loop of the cascade system plays the primary role. It is seen that the motors drive with different speeds in this stage. The relative position of the robot with respective to its target trajectory is demonstrated by the side distances S_f and S_r. In the second stage, the inner loop is saturated and e_θ is kept at its upper or lower limit and the motors operate at the same speed. The outer loop plays the leading role, and the lateral error suffers a rapid decrease to zero. Lastly, the orientation controller comes off saturation. e_θ converges to zero through the adjustment of the motor speeds. Thereafter, the robot drives in parallel to the target trajectory.

In Fig. 8, while a step signal of 1 cm is introduced to S_f as a disturbance at 40s, e_y increases from zero to 1 cm simultaneously. The trajectory controller is then activated. By adjusting the motor speeds, S_r increases drastically from its reference value to orient the robot. e_θ begins to reduce after e_y decreases to zero. Under the control effect of the guidance system, the injected disturbance is eliminated very quickly.

By comparison of simulation results in Fig. 8(a) with those in Fig. 9(a), where the tracking performances for the vehicle with the same initial position are shown, it is observed that the higher forward velocity of 0.16 m/s (in Fig. 9(a)) than that of 0.12 m/s (in Fig. 8(a)) accelerates the converging process of e_y by 7s. The converging time of the tracking error is reduced from 19s to 12s.

It is concluded that in all simulation cases the proposed controller successfully drives the robot to the desired trajectory, and an accurate row tracking is accomplished.

5.2. Experimental results

The described control structure has been implemented on the experiment platform in laboratory as is illustrated in Fig. 10. The

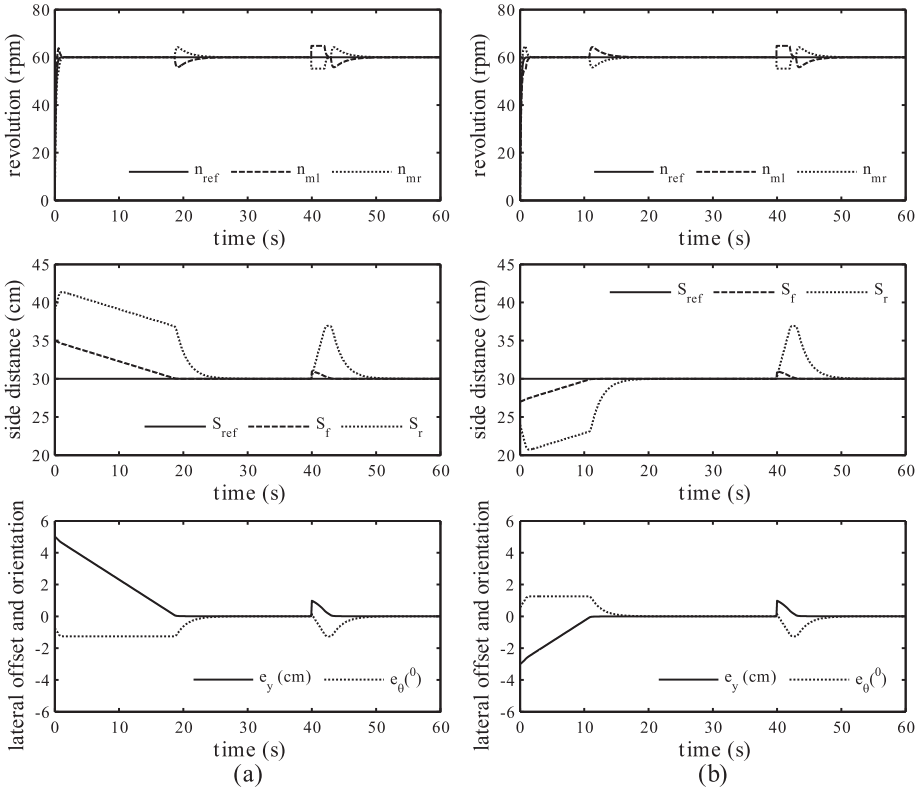

Fig. 8. Simulation results of the tracking performance for n_{ref} = 60 rpm. (a) ($e_{y0}, e_{\theta 0}$) = (5.04 cm, −1.33°), (b) ($e_{y0}, e_{\theta 0}$) = (−3 cm, 0.57°).

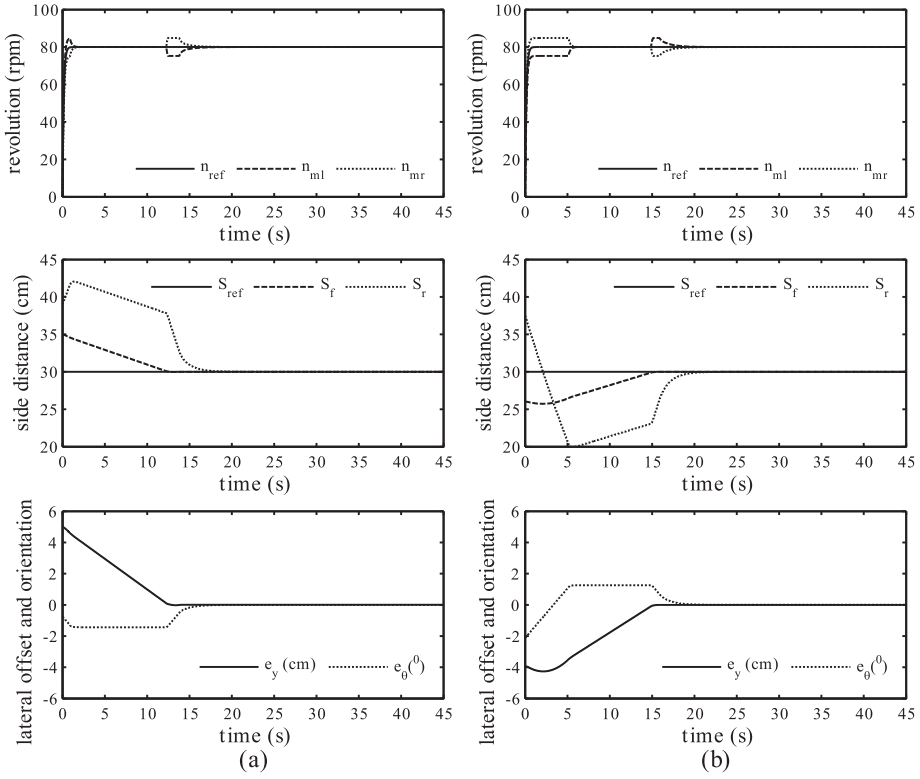

Fig. 9. Simulation results of the tracking performance for n_{ref} = 80 rpm. (a) ($e_{y0}, e_{\theta 0}$) = (5.04 cm, −1.33°), (b) ($e_{y0}, e_{\theta 0}$) = (−4 cm, −2.1°).

guidance control algorithms is programmed using LabView development environment and downloaded on a FPGA chip integrated in the NI PXI7851R module. The program is executed with a frequency of 500 Hz. The control signal provided by the PXI7851R module is connected with a Sabertooth motor driver to regulate the motor speeds. The actual motor revolution is sensed using a

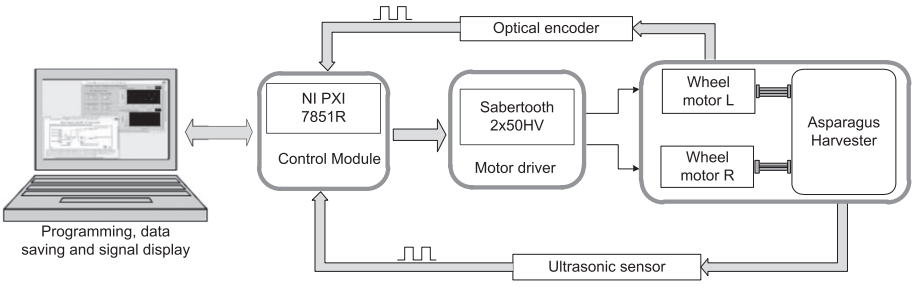

Fig. 10. Schematic illustration of the real-time experimental setup.

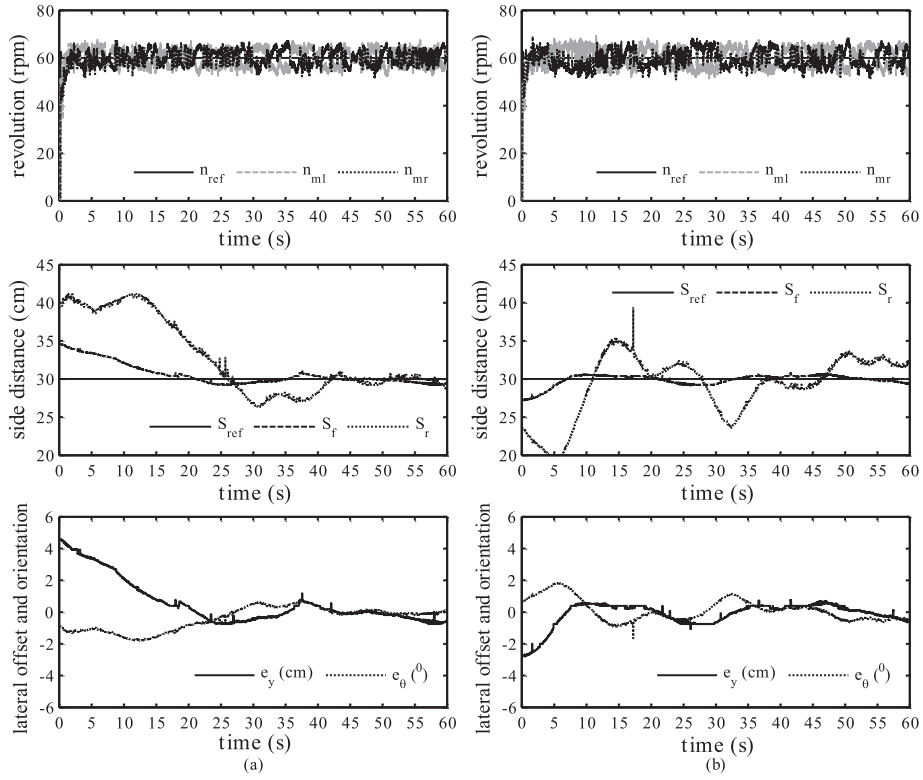

Fig. 11. Experimental results of the tracking performance for n_{ref} = 60 rpm. (a) $(e_{y0}, e_{\theta 0})$ = (5.04 cm, −1.33°), (b) $(e_{y0}, e_{\theta 0})$ = (−3 cm, 0.57°).

Model 120E incremental optical encoder, which has a resolution of 128 pulses per revolution. The side distances with respect to the target row is measured by two Parallax PING))) ultrasonic sensors which have an angular aperture of 43°. The time duration of the echo signal sensed by the ultrasonic sensor is used to calculate the actual distance. To improve the accuracy of the measured motor speeds and distances, the measuring system is performed with an execution time of 20 μs. The sensed and resulting data are saved and visualized on a computer. To allow for a fair comparison between the simulation and the experimental results, the same initial tracking errors for the mobile robot used in the simulation studies were also applied to carry out the experiments. Note that each experiment was repeated more than three times. And each time we got the similar tracking performance. The only minor difference is the response of the S_r at the startup instant due to the uncontrollable movement of the casters. One set of the experimental results are shown in Figs. 11 and 12.

It is illustrated that the experimental results agree rather well with the simulation ones. These experimental results demonstrate that with the proposed guidance control method based on cascade control, a satisfactory tracking performance with an accuracy of ±0.5 cm is achieved.

Differently from the simulation results, the motor speeds behave measuring noise and oscillation in the experimental results. This can be mainly accounted for the imperfect mechanical montage, friction of the chain gearbox and the limited resolution of the encoder. It is also observed that the rear side distance vibrates near the desired value with a maximal value of ±5 cm after S_f approaches its desired value S_{ref}. The vibration of S_r is especially evident in Fig. 11(a) due to the relative obvious lateral offset. The more evident vibration of S_r than that of S_f can be mainly explained by the large ratio of the rotate radius of the rear sensor to that of the front sensor by 3.4:1. Another cause of the vibration is the uncontrollable swing movement of the rear casters. The fluctuation of S_r at the beginning (see Figs. 11(a) and 12(a)) is due to the unmanageable initial motions of the casters.

Note that the orientation angle is stringently constrained by the lateral offset controller. The larger the operational region of the orientation angle is, the quicker the tracking error converges, but the more violently the rear part of the vehicle fluctuates, which enables the robot to run the risk in colliding with the target row or its neighbors. A compromise must be made between quickness and stability of the controlled system. The cascade control structure was proposed especially for the application of the white

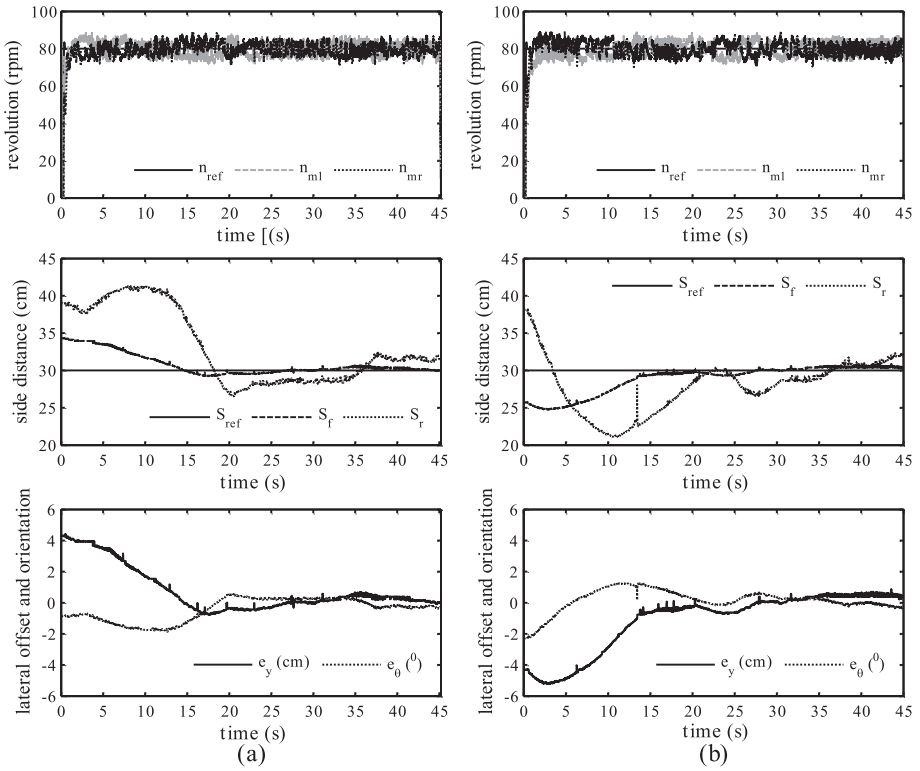

Fig. 12. Experimental results of the tracking performance for n_{ref} = 80 rpm. (a) $(e_{y0}, e_{\theta 0}) = (5.04\text{ cm}, -1.33°)$, (b) $(e_{y0}, e_{\theta 0}) = (-4\text{ cm}, -2.1°)$.

asparagus mobile robot to stabilize the robot pose during the adjustment of the tracking error, but the reported approach is not limited to the row guidance system in this work. And it has a wide applicable capability and can be applied to the differential-drive mobile robots whose heading directions are constrained due to their special working situations. The advantage of the secondary loop of the cascade control system is evident. It limits the orientation deviation with respect to the target trajectory and stabilizes the robot pose. This regulation regime is optimal for the application objective considering that the working condition of our white asparagus harvester with differential drive system. It has been verified by simulations and experiments that the fierce movement of the rear side distance is avoided, and collision-free row tracking is thus accomplished.

6. Conclusions and future work

In this paper, we have discussed a novel control strategy for the row guidance system for a differential drive field mobile robot that is developed to harvest white asparagus. The guidance system features a two-layer structure and provides the ability to reject the internal and external disturbances. Two independent speed loops at the low level have been designed to achieve stable motor speeds. A cascade control system has been suggested at the high level, which is composed of a primary lateral offset loop and a secondary orientation error loop. The cascade design allows constraints on the orientation angle to be imposed conveniently through limiting the output of the lateral offset controller. The effectiveness of the proposed control regime has been evaluated numerically and experimentally. The results show that it is effective in eliminating the initial error and tracking deviation. The most important advantage of the inner orientation control loop is that it controls directly the most significant error, which minimizes the influence of the external disturbances to the lateral offset. Therefore, the controlled system exhibits short settling time as well as excellent disturbance rejection capability. Additionally, the constraint posed upon the orientation angle has restricted the variation range of the rear side distance, which prevents effectively the robot from colliding with the asparagus bed. As a result, a satisfactory tracking performance has been achieved with high accuracy of ±0.5 cm.

In future works, the research will be deserved to improve the row guidance system by considering the dynamics of the robot and test the row guidance system of the harvesting robot in the asparagus field. Another significant task is to develop the automatic asparagus harvesting equipment, to fulfill the function of asparagus spear identification, location, cutting, holding, arrangement and so on.

References

Åstrand, B., Baerveldt, A.J., 2002. An agricultural mobile robot with vision-based perception for mechanical weed control. Autonomous Robots 13, 21–35.

Aguilar, M., Souèresm, P., Courdesses, M., Fleury, S., 1998. Robust path-following control with exponential stability for mobile robots. In: Proceedings of the IEEE Int. Conf. on Robotics and Automation, vol. 4, pp. 3279–3284.

Arndt, G., Rudziejewski, R., Stewart, V.A., 1997. On the future of automated selective asparagus harvesting technology. Computers and Electronics in Agriculture 16, 137–145.

Benson, E.R., Reid, J.F., Zhang, Q., 2003. Machine vision-based guidance system for agricultural small-grain harvester using cut-edge detection. Biosystems Engineering 86 (4), 389–398.

Borges, G.A., Lima, A.M.N., Deep, G.S., 2000. Design Of An Output Feedback Trajectory Controller For An Automated Guided Vehicle. In: Congresso de Automática, Florianó polis, Brasil, pp. 35–43.

Bonn, 2011. Knappes Angebot und hohe Preise prägten die Spargelsaison. Available from: <http://www.proplanta.de>.

Buick, R., 2006. RTK base station networks driving adoption of GPS +/−1 inch automated steering among crop growers. Agriculture White Paper.

Chatzimichali, A.P., Georgilasand, I.P.V., Tourassis, D., 2009. Design of an advanced prototype robot for white asparagus harvesting. In: Proceedings of IEEE/ASME International Conference on Industrial Advanced Intelligent Mechatronics, Singapore, 14–17 July.

Chwa, D., 2010. Tracking control of differential-drive wheeled mobile robots using a backstepping-like feedback linearization. IEEE Transactions on Systems, Man, and Cybernetics—Part A: System and Humans 40 (6), 1285–1295.

Colbaugh, R., Barany, E., Glass, K., 1998. Adaptive control of nonholonomic robotic systems. Journal of Robotic Systems 15 (7), 365–393.

d'Andréa-Novel, B., Campion, G., Bastin, G., 1995. Control of nonholonomic wheeled mobile robots by state feedback linearization. The International Journal of Robotics Research 14 (6), 543–559.

Espinosa, F., López, E., Mateos, R., Mazo, M., García, R., 2001. Advanced and intelligent control techniques applied to the drive control and path tracking systems on a robotic wheelchair. Autonomous Robots 11 (2), 137–148.

European Commission, 1999. Laying down the marketing standard for asparagus. No. 2377/1999, Commission Regulation (EC), OJ L 287, pp. 1–8.

Geyer, M., Jakob, M., Tischer, S., 2005. Partly mechanised harvest of white asparagus. Conference on Information and Technology for Sustainable Fruit and Vegetable Production, Montpellier, FRUTIC 05, pp. 183–190.

Hough, P.V.C., 1962. Method and means for recognizing complex patterns. US Patent 3 069, 654.

Kise, M., Noguchi, N, Ishii, K., Terao, H., 2002. The development of the autonomous tractor with steering controller applied by optimal control. In: Proceedings of Automation Technology for Off-Road Equipment, ASAE, Chicago, III, (USA), 26–27 July, pp. 184–189.

Klančar, G., Škrjanc, I., 2007. Tracking-error model-based predictive control for mobile robots in real time. Robotics and Autonomous Systems 55 (6), 460–469.

Leibniz-Institute of Agricultural Engineering, 2010. Case study: semi-automatic harvesting of white asparagus. Category of Agriculture, Forestry and Fishing – Crop and Animal Production, Hunting and Related Service Activities.

Li, M., Imou, K., Wakabayashi, K., Yokoyama, S., 2009. Review of research on agricultural vehicle autonomous guidance. International Journal of Agriculture & Biological Engineering 2 (3), 1–16.

Lindhout, G., 2008. Brabantse Wal presents first full-automatic asparagus harvester in the world. Available from: <http://www.freshplaza.com/>.

Marchant, J.A., Hague, T., Tillet, N.D., 1997. Row-following accuracy of an autonomous vision-guided agricultural vehicle. Computers and Electronics in Agriculture 16 (2), 165–175.

Mazur, A., 1997. Universal adaptive-tracking controller for wheeled mobile robots, In: Proceedings of the IFAC Symposium on Robot Control, pp. 33–38.

Peiter, C., 2008. Der Spargelpanther – Raubtier oder zahme Katze. Available from: <http://www.spargel-erdbeerprofi.de>.

Siegwart, R., Nourbakhsh, I.R., 2004. Introduction to Autonomous Mobile Robots. MIT Press.

Slaughter, D.C., Giles, D.K., Downey, D., 2008. Autonomous robotic weed control systems: a review. Computer and Electronics in Agriculture 61, 63–78.

Stoll, A., Kutzbach, H.D., 2000. Guidance of a forage harvester with GPS. Precision Agriculture 2, 281–291.

Tillett, N.D., Hague, T., Miles, S.J., 2002. Inter-row vision guidance for mechanical weed control in sugar beet. Computers and Electronics in Agriculture 33 (3), 163–177.

Tso, S., Fung, Y., Cheung, Y., 1996. Fuzzy logic control for differential wheel drive agvs using linear opto-sensor arrays. In: Proceedings of the IEEE Int. Conf. on Robotics and Automation, vol. 3, pp. 2816–2821.

Uwihs, F., 2008. Nicht selektiver Spargelvollernter. Available from: <http://www.spargel-erdbeerprofi.de>.

Wonneberge, C., 2005. Erntehilfen in der Spargelerte im Vergleich. Available from: <http://www.engelsmachines.nl>.

Zhang, Y., Velinsky, S., Feng, X., 1997. On the tracking control of differentially steered wheeled mobile robots. Journal of Dynamic Systems, Measurement, and Control 119 (13), 455–461.